Bimetallic Clusters by Underpotential Deposition on Layered Au Nanoparticle Films

Joohan Lee, Seongpil Hwang, Hongji Lee, and Juhyoun Kwak*

Department of Chemistry, Korea Advanced Institute of Science and Technology (KAIST), 373-1 Guseong-dong, Yuseong-gu, 305-701 Daejeon, Republic of Korea

Received: November 13, 2003; In Final Form: February 9, 2004

In this paper, we describe the well-defined underpotential deposition systems consisting of Cu, Ag, Pb, and Tl on layered gold nanoparticle (AuNP) thin films linked with bifunctional 1,6-hexanedithiol (HDT). Scanning electron microscopy informs the morphological structures of layered AuNPs accumulated by stepwise immersion in citrate-stabilized AuNP and HDT solutions. Although cyclic voltammograms for typical Au oxide formation show that colloidal AuNP frameworks are polycrystalline, (111) reflection is the major character in X-ray diffraction measurements. As the AuNP layers are piled up on indium tin oxide, faradaic currents for the underpotential deposition adsorption increase linearly, indicating that entire AuNPs are electrochemically accessible; as a result, the mass transport and the electron transfer are plausible in AuNP frameworks. Voltammetric profiles of Ag on AuNP and Cu on AuNP exhibit similar features with those on the bulk metal film. On the other hand, heavy metal systems of Pb/AuNP and Tl/AuNP reveal more enhanced adsorption currents and particularly irreversible cyclic voltammograms which explicate their strong binding properties to AuNPs by the small size of the hydrated metal ions. This electrochemical approach gives an alternative route to the construction of bimetallic clusters. The potential cycling, X-ray photoelectron spectroscopy and scanning electron microscopy demonstrate that the bimetallic cluster of Ag or Cu on AuNPs is a core−shelled shape, while the bimetallic cluster of Pb or Tl on AuNPs forms an alloyed structure.

1. Introduction

A new paradigm in the molecular or nanometer level, the so-called nanoscience or nanotechnology, which is a interdisciplinary product of fabrication, manipulation, and integration, has been emerging.[1] Among the diverse candidates for the building blocks of nanotechnology, such as fullerenes,[2] carbon nanotubes,[3−4] DNAs,[5−6] quantum dots,[7−8] dendrimers,[9] and block copolymers,[10−11] metal nanoparticles (NPs) have been recently spotlighted because they are easy to prepare, they are mostly stable, and they can be applied to catalysts,[12−14] sensors,[15−17] optical devices,[18−19] and electronic devices.[20−21]

Using the electrostatic and covalent interactions of bifunctional groups on the substrates, the assembly of individual NPs into three-dimensional ensembles has become an important and widespread research subject. Natan et al. constructed multilayered thin films with citrate-stabilized Au colloids by stepwise dipping and washing procedures in gold nanoparticles (AuNP) and 1,6-hexanedithiol (HDT) or 1,9-nonanedithiol solutions.[22] They observed through UV−vis spectroscopy that NP-modified films exhibit a linear increment of plasmon absorbance as the number of stacking layers increases. In addition, they indicated that multilayered films become conductive with a sufficient coverage of Au colloids, and that the electroactive areas were 40% to 60% larger than the electrode geometry, as verified by voltammetric measurements on several redox probes.[23−24]

Willner's group demonstrated that metal NP arrays cross-linked with molecular receptors acted as redox-active layered composites, in which NPs provided electrochemical sensing access for the redox sites of some enzymes; moreover, the AuNPs connected with photosensitizers on electron-acceptors yielded photochemistry on conductive supports.[25−26]

Turning to another viewpoint, underpotential deposition (UPD) has attracted special consideration. Defined as the electrodeposition of the monolayers or submonolayers of a foreign metal on a substrate at potentials that are more positive than the reversible or Nernst potential, UPD occurs when the adatom−substrate interaction is stronger than the adatom−adatom interaction. This phenomenon has been applied to catalysts,[27] thin films,[28] and sensors.[29]

In this study, we report a variety of characteristics of UPD events on colloidal AuNP films, selecting the representative systems of Ag, Cu, Pb, and Tl on Au. The electrochemical approach enables us to fabricate bimetallic clusters that have been mostly prepared by the solution-based synthesis.[30] The samples of Ag/AuNP and Cu/AuNP show a normal UPD phenomenon similar to the bulk Au film electrode. On the other hand, the Tl and Pb UPD on AuNPs manifest an enhanced deposition current that comes from their strong binding properties to AuNP surfaces. Interestingly, because the bimetallic clusters of Tl and Pb on AuNPs conduct their own electrocatalytic activities with respect to oxygen reduction,[31] they play a prominent role in the oxygen catalysis of fuel cells. Potential cycling, X-ray techniques, and scanning electron microscopy (SEM) measurements indicate that the bimetallic clusters of Ag/AuNP and Cu/AuNP have core−shelled structures while those of Tl/AuNP and Pb/AuNP form alloyed structures.

2. Experimental Section

Materials. For the substrate, we used glass coated with indium tin oxide (ITO) (Samsung Corning, < 30 Ω), which did not show the UPD phenomenon in the given systems. In

* Corresponding author. Fax: +82-42-869-2810. E-mail: Juhyoun_Kwak@kaist.ac.kr.

10.1021/jp037460+ CCC: $27.50
Published on Web 04/03/2004

SCHEME 1: Illustrative Cartoon for the Modification of ITO Substrates and Representative Bimetallic Structures after Metal Underpotential Deposition.

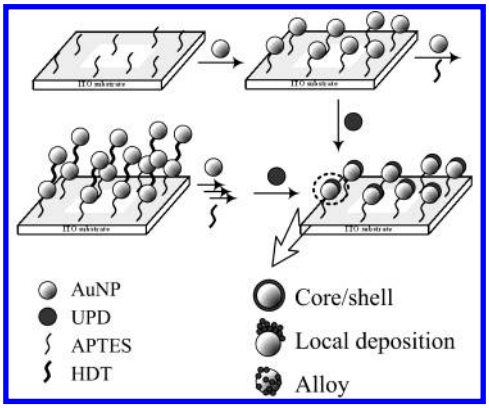

accordance with a published procedure, the working electrode for the control experiment was an Au(111) single crystal (MaTeck, Germany) annealed for 3 min in a hydrogen flame before use and slowly cooled in air.[33] The geometrical electrode area of the ITO was 0.246, while that of Au(111) was 0.785 $cm.^2$ The following chemicals, which were purchased from Aldrich, were used without further purification: $HAuCl_4 \cdot 3H_2O$, Na_3-citrate, HDT, 3-aminopropyl)triethoxysilane (APTES), Ag_2SO_4 (99.999%), $CuSO_4 \cdot 5H_2O$ (99.999%), $TlNO_3$ (99.999%), $Pb(ClO_4)_2 \cdot xH_2O$ (99.995%), $HClO_4$ (double-distilled), H_2SO_4 (99.999%). Stock solutions for electrochemistry were prepared from ultrapure water (Modulab, US Filter, MA, > 18 MΩ).

Synthesis. Colloidal AuNPs were synthesized by citrate reduction of $HAuCl_4$ as described in the literature;[34] all the glassware was thoroughly cleaned in Nochromix (Fisher) overnight and rinsed in deionized water before use. A solution of 39.38 mg of $HAuCl_4 \cdot 3H_2O$ dissolved in 100 mL H_2O was placed in a 250 mL round-bottomed flask equipped with a reflux condenser and a magnetic stirring bar. We moderately injected 10 mL of 38.8 mM citrate solution into the refluxed solution and kept stirring for more than 15 min after the color of the solution changed to deep red. The resulting solution showed a distinctive plasmon absorption peak at 520 nm, and transmission electron microscopy (TEM) manifested 13 ± 2 nm-sized AuNPs.

Preparation of AuNP Films. We constructed monolayered or multilayerd AuNP films by the alternate accumulation of AuNPs and HDT molecules, in accordance with the literature.[32] ITO substrates were pretreated in the 10% ethanolic APTES solution for a day after they were alternately cleaned in acetone and H_2O. Silanized-ITO substrates were immersed in 1 mM colloidal Au solutions for 6 h and in 5 mM ethanolic HDT as a cross-linker for 3 h from the second layer; in the middle of each step, ITO electrodes were exhaustively washed with absolute ethanol and deionized water. The procedure is illustrated in Scheme 1. The AuNP-multilayered films on ITO exhibited a distinct wine-like color that deepened as the AuNPs accumulated. Under the electrochemical deposition of UPD metals on AuNPs, at least three possible shapes were found in the structures of bimetallic clusters: core−shelled, locally deposited, and alloyed particles. Using HDT as a cross-linker, rotating disk electrodes (RDE) with monolayered AuNP films were modified on polycrystalline Au with a diameter of 3 mm.

Electrochemical Measurements. Cyclic voltammetry was performed with a Pt counter electrode and a mercury−mercurous sulfate reference electrode connected to an electrochemical cell via a capillary salt bridge to reduce contamination. All potentials

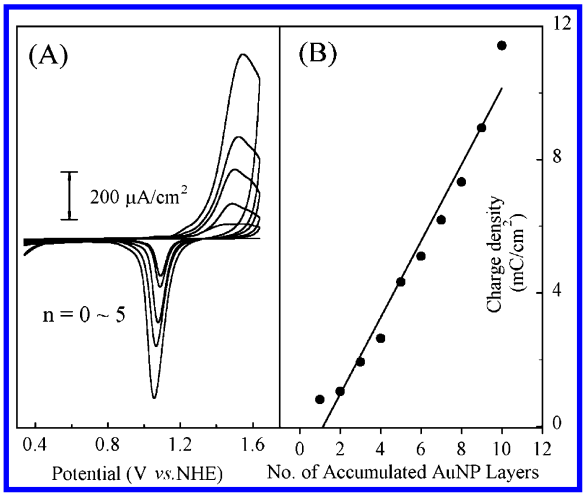

Figure 1. Cyclic voltammograms of APTES-modified ITO and mono- to five-layered AuNP films in 0.1 M $HClO_4$ electrolytes at 20 mV/s (a) and the corresponding charge density plot (b).

in this paper, however, are quoted with respect to a normal hydrogen electrode (NHE). The solutions were purged with argon before use, and the Ar atmosphere was maintained during all measurements. Potential control and sweeps were conducted with an Autolab potentiostat (PGSTAT 10, EcoChemie, Netherlands). RDE measurements were obtained using a BAS model RDE-1 rotator (Bioanalytical Systems, IN).

Instrumentation. Field emission-SEM images were collected on a scanning electron microscope (Philips XL30SFEG), in which the electron gun was set to 10 kV. X-ray diffraction (XRD) measurements were conducted on an X-ray diffractometer (Rigaku, D/MAX-RC) using Cu Kα radiation. The angle of 2θ was scanned from 20° to 80° with a scan speed of 3.0°/min. X-ray photoelectron spectroscopy (XPS) was obtained with an X-ray photoelectron spectrometer (PHI Model 5800, Phys. Elec. Inc.).

3. Results and Discussion

Figure 1 shows cyclic voltammograms (CVs) on AuNP-modified ITO electrodes cross-linked with HDT in 0.1 M $HClO_4$ solutions and the charge graph for cathodic sweeps as the AuNP layers increase. A broad peak coming from the oxide formation of AuNPs starts to emerge around 1.2 V, and the corresponding typical cathodic peaks are also observed.

Normally, single-crystal electrodes exhibit sharp anodic peaks split with several components, depending on the crystal orientation of a substrate. Consequently, the AuNP films are polycrystalline: their components have (100) and (111) planes on the basis of the geometric shape by the synthetic route. XRD measurements, however, indicate that AuNP films covalently attached to the ITO substrate mainly hold a (111) reflection similar to the evaporated Au film electrode (see Figure 2). The charge density associated with the reductive process is 0.804 mC/cm^2 for the first AuNP layer, as shown in Figure 1(b). This result denotes that the electrode area of the AuNPs connected with APTES on ITO is 1.7 times higher than the planar Au(111) electrode (0.462 mC/cm^2).[35] Assuming that all of the AuNP surfaces are involved in the electrochemical reaction, the surface coverage of the AuNPs is estimated to be 3.3×10^{11} particles/cm^2, which is similar to the literature[36] and to the following SEM image in this paper. For the stability and facility of film preparation, bifunctional HDT molecules, of which the resistance is approximately 10 MΩ corresponding to the electron-transfer rate of 1.0×10^{-5} along their carbon chains, are employed from

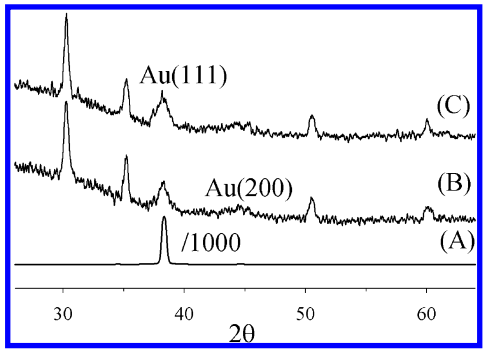

Figure 2. XRD patterns of evaporated Au films on glass, followed by annealing processes (a), five-layered AuNPs before (b), and after electrochemistry (c).

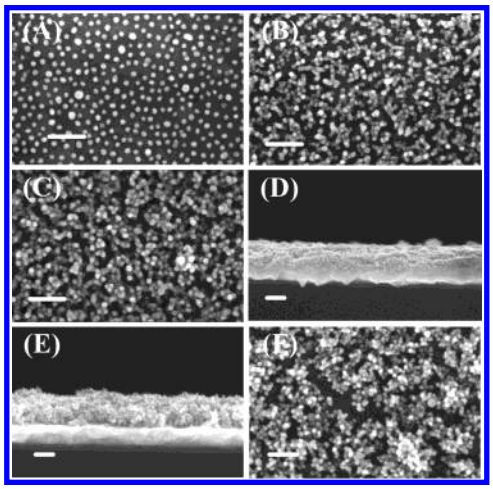

Figure 3. SEM images of AuNP-modified ITO surfaces. Top-view images over mono- (a), three- (b), and five- (c) layered AuNP films. Side-view images of six- (d) and nine- (e) layered AuNPs. Five-layered AuNPs after the electrochemistry (f). Scale bar: 100 nm.

the second modification.[37,38] The charge density plot shows a linear increment as the AuNP layers are accumulated, indicating the electrochemical accessibility to all the AuNPs. The introduction of HDT molecules in the linkage of AuNPs consequently presents no problem in the transfer of electrons.

The cross-linker molecules are undoubtedly stable during and after potential sweeps. As shown in Figure 2(c), the XRD pattern of AuNP films after electrochemical measurements shows the same profile as the primitive five-layered AuNP film. In addition, the SEM image in Figure 3(f) indicates that AuNP films keep their initial texture during electrochemical experiments. On the basis of these kinds of results, we conclude that APTES or HDT is not oxidatively desorbed under this potential range, and the charge values in Figure 1(b) only result from the Au component. Therefore, individual AuNPs serve as a robust nanoelectrode on stepwise-constructed AuNP thin films.

Figure 2 displays XRD patterns of Au evaporated on glass with a Cr-adhesion layer purchased from Metallhandel Schröer GmbH, followed by annealing procedures (a), layered AuNP films on ITO fabricated by five alternate immersions in AuNP and cross-linker solutions before (b), and after an electrochemical experiment (c) under the radiation of Cu Kα. The reference data reveal that the lattice parameters of Au(111) and Au(200) emerge at 38.184° and 44.392°.[39−40] These values are identical with the profiles of the evaporated Au films. Although the peak of the five-layered AuNP film is less sharp than the peak shown in Figure 2(a), a considerably strong (111) peak and a weak (200) peak appear at the same angles with the evaporated Au, implying that AuNP films are substantially equivalent to the properties of the Au film substrate. Other peaks at 30.27°, 35.16°, 51.00°, and 59.94° indicate (222), (400), (441), and (622) reflections of the ITO substrate, respectively.[41] According to the literature, a polished polycrystalline gold disk exhibits a variety of peaks, namely (111), (200), (220), and (311), and also other peaks are relatively stronger than (111).[42] We therefore deduce that the accumulated AuNP films hold a more excellent quality of crystal orientation than a polycrystalline gold disk electrodes though the AuNP films are inferior to the quality of the annealed Au film substrate.

SEM measurements powered with a 10 kV electron source visualize the surface coverage and morphologies of AuNP-modified ITO electrodes, as shown in Figure 3. The three top-view images consist of one, three, and five AuNP layers, while the two side-view images consist of six and nine layers. As observed in the electrochemical experiments, the SEM images also reveal the linear increase of AuNP density.

In the case of the first layer with the cross-linker of APTES, as shown in Figure 3(a), 380 AuNPs occupy the given image, corresponding to a surface coverage of 1.7×10^{11} particles/cm^2. The surface coverage closely matches that of the charge density calculation as mentioned above. Even if the immersion time is prolonged, the surface is not fully covered with AuNPs. This phenomenon is caused by the repulsive forces between the AuNPs with negative charges of citrates and the roughness of the base ITO electrode. Consequently, the construction of a compact monolayer coverage requires a smooth substrate and neutral colloids. Figure 3(b) and Figure 3(c) show the microstructure of three- and five-layered AuNP thin films. The popularity of the AuNPs proportionally increases keeping small pores among the interconnected AuNPs as the dipping cycles are repeated. To gain further information on the AuNP frameworks, we executed alternate immersion procedures for up to 30 layers (the results of which are not shown here). The corresponding SEM image displayed large pores (up to 10 μm) and defects built by the interconnection of AuNP-assembled structures. The pores and defects could play an important role in the passage of ions and redox molecules. The vertical height of multilayered AuNPs is more lucidly visualized on side-view images. Figure 3(e) shows nine-layered AuNPs with a thickness of 150 ± 20 nm. This result shows that AuNP films have a layer-by-layer structure accumulated by alternate dipping and washing of the substrates.

Figure 4 shows voltammetric responses and the corresponding charge density plot on AuNP films in 0.1 M H_2SO_4 containing 1 mM $CuSO_4$ at 5 mV/s. An Au(111) single crystal was selected as a standard for comparison with UPD features on AuNP-modified ITO. As indicated in the literature, the uppermost CV, the Cu UPD on Au(111), is composed of two well-defined pairs of peaks, which are assigned to two different adsorption−desorption processes.[43] The first pair of sharp peaks corresponds to the $(\sqrt{3} \times \sqrt{3})$ adlayer structure, and the second pair of peaks corresponds to the (1×1) transformation. To determine whether Cu can be underpotentially deposited on the ITO substrate, the Cu was deposited on only APTES-treated ITO (the second CV, solid line), which shows no cathodic or anodic trace. We therefore deduce that the Cu deposition only on AuNPs generates the voltammetric appearances within the given potential ranges.

The third CV (dashed line) with two broad peaks during reductive sweeps depicts the Cu UPD on monolayered AuNPs. A broad peak starts to emerge at 0.53 V, and another peak appears around 0.25 V, implying that the Cu deposition on AuNPs possesses two thermodynamic energy states. Compared

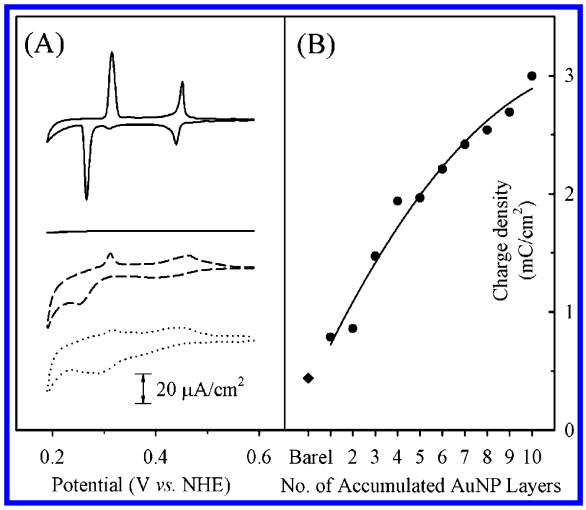

Figure 4. Cyclic voltammograms on layered AuNP films in 1 mM $CuSO_4$ + 0.1 M H_2SO_4 solutions at 5 mV/s (a). The Cu UPD on a Au(111) single crystal (the topmost curve), on APTES-modified ITO (solid line), on monolayered AuNPs (dashed line), and on two-layered AuNPs (dotted line). The corresponding charge density plot (b) on Au(111) (diamond) and one- to ten-layered AuNPs (circles).

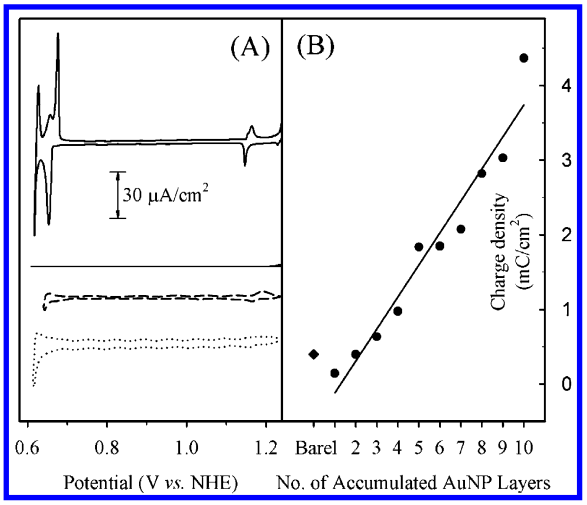

Figure 5. Cyclic voltammograms on layered AuNP films in 1 mM Ag_2SO_4 + 0.1 M H_2SO_4 solutions at 5 mV/s (a). The Ag UPD on a Au(111) single crystal (the topmost curve), on APTES-modified ITO (solid line), on monolayered AuNPs (dashed line), and on two-layered AuNPs (dotted line). The corresponding charge density plot (b) on Au(111) (diamond) and one- to ten-layered AuNPs (circles).

with the Au(111) system, the UPD peak potentials at cathodic scans are difficult to determine the UPD peak potentials because the peaks are broadened and the peak potentials shift negatively, which are associated with the slow kinetics of the metal deposition on self-assembled monolayers.[44−46] However, the anodic peak potentials and shapes for the Cu dissolution become evident. Using a "place exchange" reaction to easily modify AuNPs, the cross-linker is replaced with HDT from the second layer.[47] The fourth CV (dotted line) on the Cu UPD on two-layered AuNPs is nearly analogous to that on monolayered AuNPs except for the enhancement of deposition and stripping currents because of the increase in the effective surface areas and the shift of the second cathodic peak toward a positive direction. The Cu UPD features on multilayered AuNPs are included in the Supporting Information (see Figure S1).

The coulometric charge density, subtracted from the value of background charging current based on only APTES-modified ITO, of the Cu UPD on monolayered AuNPs is 776 $\mu C/cm^2$ for the reductive profile, which is 1.8 times higher than that on a planar Au(111) electrode (440 $\mu C/cm^2$), as shown in Figure 4(b). This result means that the electrode area of monolayered AuNP films increases 80%. If the potential and deposition time are appropriately chosen in the given system, the electrochemical method affords another route to the fabrication of bimetallic clusters. They improve catalytic activities of original single-metal catalysts and create a new property generated from an ensemble or a ligand effect in catalyses.[48]

Weaver's group applied the Cu UPD on AuNPs to the construction of transition metal-coated NP films, using galvanic exchange processes.[49] The Pt or Pd-shelled particles exhibited representative traits of oxide formation, marking them more effective candidates for CO oxidation catalysts.[50] Electrochemistry therefore offers a pathway to monitoring deposition events[51,52] and to establishing bimetallic colloids on a conductive support by UPD phenomena. The synthetic methods of these phenomena have been principally divided into two categories: "co-reduction" and "successive reduction." The two categories produce alloyed or core−shelled particles.[30]

Figure 5 displays voltammetric responses and the corresponding charge plot of Ag UPD on AuNP films in 0.1 M H_2SO_4 electrolytes that contain 1 mM Ag_2SO_4 at a scan rate of 5 mV/s. For a comparison, we performed a voltammetry of the Ag UPD on a Au(111) single crystal, and the result is shown in the topmost CV. We can observe two pairs of Ag deposition and stripping peaks and smooth charging current regimes consistent with the literature.[53−54] No distinctive feature appears in the second CV (solid line) of Ag UPD on APTES-treated ITO within the given potential range, validating that Ag adsorbs only on AuNPs.

The third and fourth CVs (dashed and dotted lines) exhibit a pair of peaks around 1.2 V and a broad peak before the bulk deposition. The first UPD peak is clearly observed, whereas the second one does not become visible. Because the second UPD peak before the bulk deposition depends on the crystallinity of an electrode, AuNP films constructed by alternate accumulation have fewer ordered properties than Au(111). These properties, however, are better than those of a polycrystalline Au electrode, as shown by XRD studies in Figure 2.[55] In addition, the Supporting Information section includes the Ag UPD features on multilayered AuNP films (see Figure S1).

From another viewpoint, in the CVs on mono- and bilayered AuNP films, eye-catching wavy peaks appear in the charging current regions. Murray et al. described this phenomenon as "quantized double layer (QDL) charging," it occurrs when the effective capacitances of AuNPs are so small that single electron changes in their core charges arise at large voltage intervals, even at room temperature.[56]

In contrast to the work of Murray et al. on solution-based systems by differential pulse voltammetry, our research discloses that the QDL events emerge on layered films of citrate-stabilized AuNPs in the regime of the potential of zero charge by CV measurements. Detailed studies are in progress. As with other UPD, adsorption currents show a linear increase as AuNPs are stacked up. This phenomenon is more clearly seen in the charge density plot in Figure 5(b). The charge density on low AuNP layers becomes smaller than that on Au(111), as a result of the disappearance of the second UPD peak though the charge values overwhelm the charge density of bare Au(111) from three-layered AuNPs.

Figure 6 shows CVs and the corresponding coulometric charge density of Tl on AuNP layers in 0.1 M $HClO_4$ containing 1 mM $TlNO_3$ at 5 mV/s. The uppermost CV displays Tl UPD

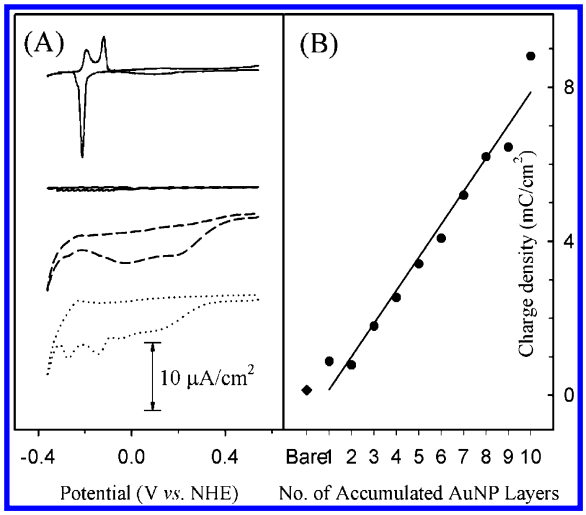

Figure 6. Cyclic voltammograms on layered AuNP films in 1 mM $TlNO_3$ + 0.1 M $HClO_4$ solutions at 5 mV/s (a). The Tl UPD on a Au(111) single crystal (the topmost curve), on APTES-modified ITO (solid line), on monolayered AuNPs (dashed line), and on two-layered AuNPs (dotted line). The corresponding charge density plot (b) on Au(111) (diamond) and one- to ten-layered AuNPs (circles).

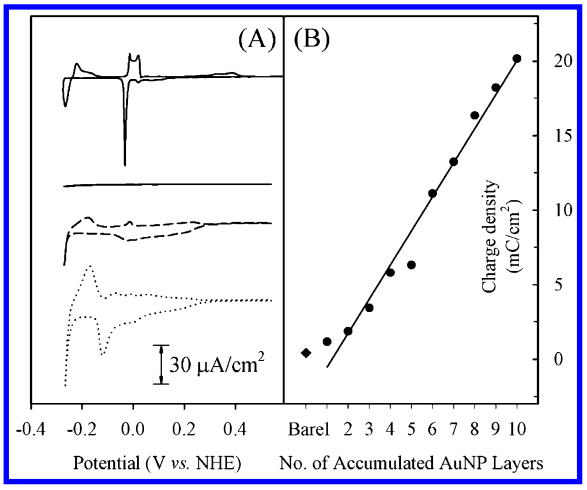

Figure 7. Cyclic voltammograms on layered AuNP films in 1 mM $Pb(ClO_4)_2$ + 0.1 M $HClO_4$ solutions at 5 mV/s (a). The Pb UPD on a Au(111) single crystal (the topmost curve), on APTES-modified ITO (solid line), on monolayered AuNPs (dashed line), and on two-layered AuNPs (dotted line). The corresponding charge density plot (b) on Au(111) (diamond) and one- to ten-layered AuNPs (circles).

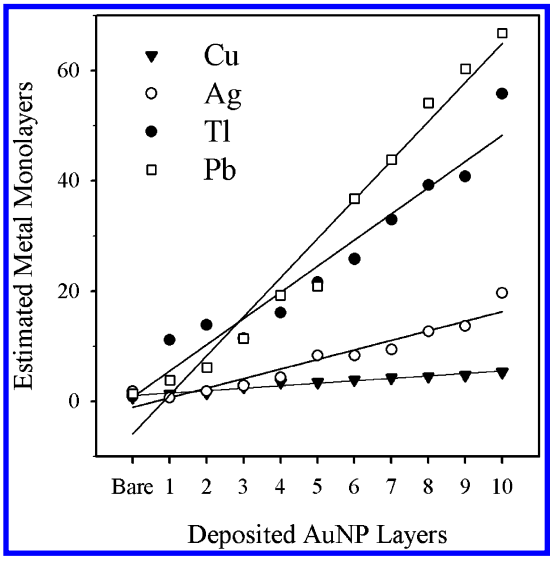

Figure 8. Scatter plots for the amount of underpotentially deposited metal on colloidal Au layers based on charge density values.

on Au(111). As previously reported, the CV is composed of a sharp cathodic peak and an anodic peak split into two components.[57] The Tl deposition was performed on only APTES-treated ITO (the second CV, solid line), in which no cathodic/anodic trace (only charging current) appears. We therefore deduce that the Tl deposition only on AuNPs generates the voltammetric appearances within the given potential ranges. Compared with a Tl on Au(111) system, CVs of Tl on AuNPs show the following features:

•UPD processes begin at 400 mV more positive than that on Au(111) (dashed line).

•Multiple adsorption peaks emerge but the Tl desorption almost fails to occur (dotted line).

•The charge density of Tl on AuNPs has approximately a 10-fold increase.

Although voltammetric traces are poorly defined as AuNPs are accumulated, these findings suggest that Tl atoms tend to bind strongly with AuNPs. This phenomenon is corroborated with voltammetric potential cycling, in which CV profiles show decreased currents in the second cycle because of the reduced electrode areas caused by Tl occupancy in the first cycle (see Figure 9). For a CV on five-layered AuNPs, the Tl adsorption current starts to increase at 0.4 V and two adsorption peaks appear at around −0.2 V; the charge density value is 3.42 mC/cm^2, which corresponds to about 20 Tl metallic monolayers on AuNPs (see Figure S1). This overwhelmingly enhanced current of Tl on AuNPs could act as an electrocatalytic assistant because Tl or Pb on Au(111) shows a catalytic oxygen reduction.[31] We are presently applying these observations to real catalysts. The charge density plot for each AuNP layer is shown in Figure 6(b), and the linear increment of Tl adsorption charges on AuNPs is observed as the AuNP layers increase.

Figure 7 shows the voltammetric profiles and the corresponding charge plot for cathodic sweeps of Pb on AuNPs in 0.1 M $HClO_4$ containing 1 mM $Pb(ClO_4)_2$ at 5 mV/s. As previously reported, the CV of the Pb UPD on an Au(111) single crystal (the topmost curve) exhibits a sharp cathodic peak at −0.03 V, and the corresponding anodic peaks are divided into two components.[58] In the positive potential region, charge consumption is associated with the bump formation at step-edges (step decoration). No Pb UPD on APTES-modified ITO is shown in the second CV (solid line), demonstrating that the Pb UPD occurs only on AuNPs in other CVs. The third CV (dashed line) indicates the profile of the Pb UPD on monolayered AuNPs.

Although the cathodic and anodic peaks are less sharp than those of Pb on Au(111), the position of peak potentials distinctly coincides with the peaks of the Au(111) case, connoting that the cross-linker, APTES, does not severely obstruct the Pb adsorption on AuNPs. On the other hand, the CV (dotted line) with the cross-linkers of HDT molecules yields overpotentials with as much as −100 mV shifts stemming from thiol groups that block the penetration of Pb atoms toward HDT-modified gold surfaces.

Analogous to the Tl UPD on AuNPs as described above, electrochemical measurements of Pb on AuNPs reveal several particular configurations:

•UPD processes begin at substantially positive potentials.

•As the number of AuNP layers increases, the profiles of Pb adsorption are split into two peaks at −0.01 V and −0.14 V, while the profiles of Pb desorption are merged into one peak at −0.08 V.

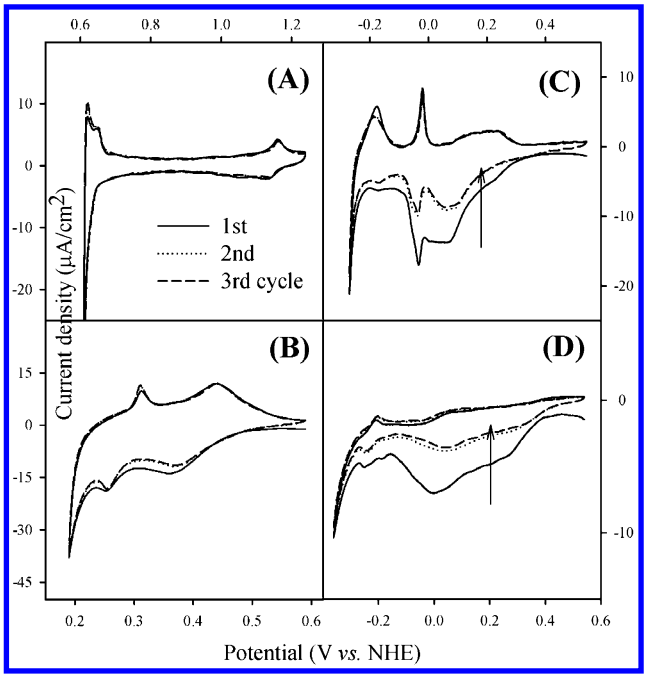

Figure 9. Consecutive potential cycling of Ag (a), Cu (b), Pb (c), and Tl (d) UPDs on monolayered AuNPs. Scan rate = 5 mV/s.

•Compared with a Pb on Au(111) system, the charge plot reveals that the amount of metallic Pb monolayers on AuNPs increases steeply; for example, the Pb UPD on five-layered AuNPs conforms to 20 monolayers.

Because the Pb UPD is also capable of oxygen reduction, the intense properties of the Pb atoms adhering to Au surfaces will be applicable in future electrocatalysis. In addition, the charge density values for the cathodic sweeps in Figure 7(b) disclose a linear increase as AuNPs are deposited. The charge density of Pb on Au(111) is allotted 1.4 monolayers, whereas the charge density of Pb on ten-layered AuNPs corresponds to roughly 65 monolayers. This 5-fold increase is a result of the alternately accumulating AuNPs and cross-linkers.

Focusing on the stabilizing agents and cross-linkers during the electrochemical deposition, we perceive that two possible structures can be assumed when underpotentially deposited metals adsorb on AuNPs:

•The deposited metal sits on the tail of thiol or citrate molecules.

•The UPD metal penetrates into the space between Au surfaces and cross-linkers, forming an Au/ UPD metal/linker structure.

In the literature, the second model was reasonable in the systems of Ag and Cu UPD on alkylthiol-modified Au(111).[59] To determine whether this observation can be applied to the UPD on AuNPs, we performed SEM measurements on layered colloidal AuNPs. If the first assumption is true or self-assembled monolayers are dissembled during and after the metal deposition, surface morphologies can be agglomerated. However, the SEM images indicate that AuNP films keep their initial texture after UPD experiments (not shown here). Therefore, the reassembly of thiol groups with UPD metals arises during metal adsorption on AuNPs.

Figure 8 shows multiple plots for AuNP layers in contrast to the estimated metallic monolayers based on the charge measurements for cathodic sweeps in order to determine the amount of metal deposited on the AuNPs. A monolayer of Ag, Cu, Tl, and Pb on Au(111) requires a charge density of 222 μC/cm^2, 565 μC/cm^2, 158 μC/cm^2, and 302 μC/cm^2, respectively, under

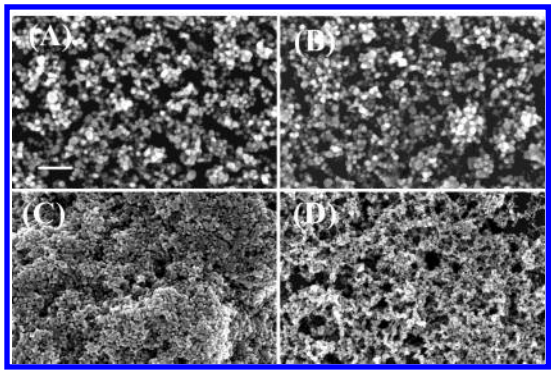

Figure 10. SEM images after the construction of bimetallic clusters on five-layered AuNP films. Cu/AuNP (a), Ag/AuNP (b), Tl/AuNP (c), and Pb/AuNP (d). Scale bar: 100 nm.

the assumption that each underpotentially deposited metal is commensurate with the (111) plane of AuNP surfaces, and a hexagonally close packing structure is formed. For Pb and Tl on AuNPs, a sharp augmentation of metallic monolayers occurs, though the salient enhancement does not appear in the Cu case. The driving force of this tendency appears to be the smaller size of the hydrated metal ions, which can more easily penetrate into the AuNP framework and cross-linkers. According to the literature, the Stokes radius, which is constituted by the valence number of the ion and infinite molar conductivity, increases in the order of Tl < Pb < Ag < Cu.[60] Considering the size of the hydrated ions, the plot of Figure 8 is reasonable.

Determining the structure of bimetallic clusters on AuNP films is important. The first step is to obtain information on the voltammetric cycling for individual UPDs on the monolayered AuNPs on ITO, as shown in Figure 9. All the CVs have similar features with UPDs on Au(111) even though they exhibit peak broadening. For Ag/AuNP and Cu/AuNP, no changes occur in the voltammetric appearances and current scales regardless of how the potential cycling is repeated.

In Weaver's reports, the Cu UPD on AuNPs was used to make a Pt−Au core−shelled structure as a galvanic exchanging agent.[61] Murray et al. also described a synthesis of bimetallic structures; they used the galvanic replacement in which the transformation from initial nucleation to a core−shelled structure on thiol-protected gold clusters was revealed in the UV−visible spectra.[62]

On the other hand, the current values of Pb/AuNP and Tl/AuNP decrease over several potential cycles. We can easily speculate that because the stripping peaks are relatively small the reduced adsorption currents stem from the decreased electrode area by the pre-residence of deposited metals (Pb or Tl) on AuNPs during the first sweep. On the basis of these results, the bimetallic clusters of Pb/AuNP and Tl/AuNP could become alloyed because the desorption of alloys normally requires more overpotential. To obtain the information on the stability of monolayered AuNP frameworks under the easy supplies of metal ions, potential cycling on RDEs were conducted (mass-transfer control) (see Figure S2). All the voltammetric features are similar to those at the stationary electrode systems. This result consequently reconfirms the stability of AuNP films during electrochemistry and the above statements. The following SEM and XPS data will also support these observations.

Figure 10 shows SEM images after the construction of bimetallic clusters with a monolayer of UPD metals. Interestingly, no change is observed in the Ag/AuNP and Cu/AuNP, whereas Tl/AuNP and Pb/AuNP exhibit the agglomeration among metal deposited AuNPs. Holding the initial morphology

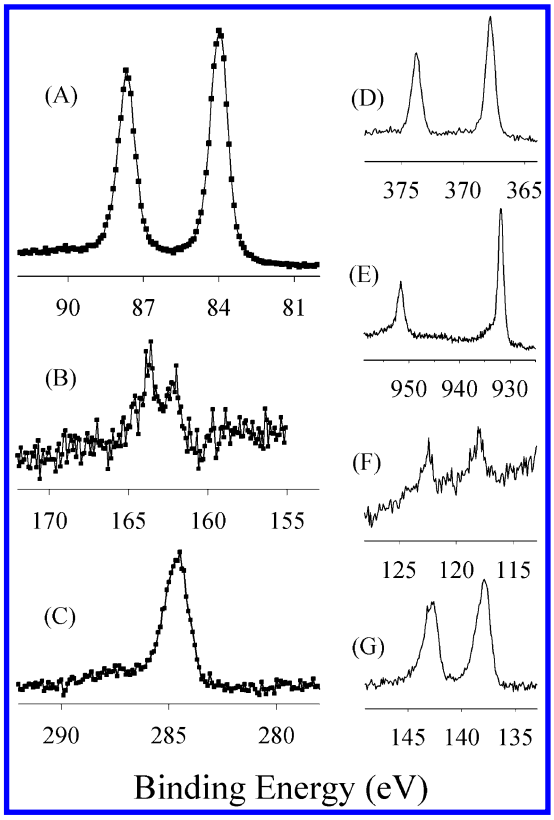

Figure 11. XPS of Au4f (a), S2p (b), and C1s (c) realms over five-layered AuNP films. The apparent spectra of Ag4d (d), Cu2p (e), Tl4f (f), and Pb4f (g) components on the bimetallic clusters fabricated by electrochemistry.

of the AuNP films after the metal deposition indicates that Ag or Cu atoms are wrapped on AuNP surfaces as metal ions smear into the space between the AuNP and the cross-linker. The bimetallic clusters of Tl/AuNP and Pb/AuNP, however, show the fusion of the framework. The fusion comes from the change in assembled structures or the removal of the capping molecules, intimating that Tl or Pb atoms are intermixed with Au atoms. Hence, there is a probability that Tl/AuNP and Pb/AuNP become alloyed particles.

To observe the stability of bimetallic clusters and whether they were fabricated by electrochemical approaches, we conducted XPS measurements on individual metal UPDs on AuNP films constructed by a 5-fold modification of ITO as shown in Figure 11. Initially, we focused on the stability of the frameworks caused by AuNPs and cross-linkers after inducing electrochemical potentials. The spectra reveal that the binding energies (BE) of $Au4f_{7/2}$ (a), $S2p_{3/2}$ (b), and C1s (c) appear at 84.0, 163.0, and 284.6 eV, respectively, closely matching the reference values. In particular, the spectra of S2p (from HDT molecules) and C1s (from citrates and HDT) clarify that the morphologies of layered colloidal Au films are preserved during and after UPD processes. Moreover, Figure 11 provides the BEs of the surface atomic compositions of Ag4d (d), Cu2P (e), Tl4f (f), and Pb4f (g) photoelectron spectra for each metal UPD that is voltammetrically swept before the bulk deposition potentials on five-layered AuNPs on ITO electrodes. The peaks for $Ag4d_{5/2}$, $Cu2p_{3/2}$, $Tl4f_{7/2}$, and $Pb4f_{7/2}$ peaks emerge at 367.8, 931.9, 118.0, and 138.0 eV, respectively, and their differences to the BEs relative to the bulk values of each metal, ΔE, are -0.5 eV, -0.8 eV, $+0.3$ eV, and $+1.1$ eV.[63]

Interestingly, the BEs of Ag and Cu shift toward the negative direction, while the BEs of the heavy metals Tl and Pb shift toward the positive. According to one study, the alteration of BEs comes from alloying (ΔE_a) and the effects of cluster size (ΔE_c) in the bimetallic clusters.[64] In our systems, ΔE_c can be negligible because the size of the mother metal, Au, is presynthesized to be 13 nm in our systems. For mole fractions, the metal with the lower value in the composition of bimetallic clusters normally exhibits the negative movement of BEs. Furthermore, the previous XPS measurements on underpotentially deposited metal show the negative shifts of BEs relative to the bulk metal.[27] The negative BE changes in the Ag and Cu UPD can be rationalized by the small mole fraction of UPD metals and the inherent character of the UPD. In particular, the positive shifts in Tl and Pb are influenced by ΔE_a. Thus, we conclude that the bimetallic clusters of Ag/AuNP and Cu/AuNP have a core−shelled structure, whereas those of Tl/AuNP and Pb/AuNP form an alloyed shape. These agree well with the results of the potential cycling and SEM measurements.

4. Conclusions

We performed electrochemical measurements on various UPD systems to confirm their distinct features and voltammetric sweeps to construct bimetallic clusters on layered AuNPs linked with dithiol groups. SEM images describe the complete morphologies for the AuNP frameworks. In these frameworks, the electrostatic repulsion between citrate-modified AuNPs produces open spaces and, occasionally, large pores that provide the pathways for mass transport. This process demonstrates that electrochemical accessibility is a possibility for all the Au clusters, leading to the linearity of the adsorption currents for each metal system because of the accumulation of colloidal AuNPs. In addition, XRD patterns supported by SEM and XPS measurements show that AuNP films explicitly exhibit (111) characteristics and maintain their networks during and after voltammetric sweeps.

We also fabricated bimetallic clusters on a conductive solid support. Potential cycling, SEM, and XPS measurements verify that Ag/AuNP and Cu/AuNP have a distinctive core−shelled structure, whereas Tl/AuNP and Pb/AuNP are designated with an alloyed structure. With respect to electrocatalysis, particular concerns can be provoked in the Tl/AuNP and Pb/AuNP systems with electrocatalytic activities in the oxygen reduction because alloys have advantages in plentiful and regularly distributed active sites. Currently, we are studying Tl/AuNP and Pb/AuNP as an alternative for the precious catalysts Pt and Pd.

Acknowledgment. This work was supported by the Korean Ministry of Science and Technology through the National R&D Project for Nano Science and Technology. We also gratefully acknowledge the partial support from the Brain Korea 21, MICROS, and IMT 2000 projects.

Supporting Information Available: CVs of metal UPDs on the multilayered AuNP films (Figure 1S.). Consecutive potential cycling for individual UPDs on monolayered AuNP-modified RDEs (Figure 2S). This material is available free of charge via the Internet at http://pubs.acs.org.

References and Notes

(1) Stix, G. *Sci. Amer*. **2001**, *Sept.*, 32.
(2) Sawamura, M.; Kawai, K.; Matsuo, Y.; Kanie, K.; Kato, T.; Nakamura, E. *Nature* **2002**, *419*, 702.
(3) Ajayan, P. M. *Chem. Rev*. **1999**, *99*, 1787.
(4) Postma, H. W. Ch.; Teepen, T.; Yao, Z.; Grifoni, M.; Dekker: C. *Science* **2001**, *293*, 76.
(5) Braun, E.; Eichen, Y.; Sivan, U.; Ben-Yoseph, G. *Nature* **1998**, *391*, 775.
(6) Storhoff, J. J.; Mirkin, C. A. *Chem. Rev*. **1999**, *99*, 1849.

(7) Markovich, G.; Collier, P.; Henrichs, S. E.; Remacle, F.; Levine, R. D.; Heath, J. R. *Acc. Chem. Res.* **1999**, *32*, 415.
(8) Wang, C.; Shim, M.; Guyot-Sionnest, P. *Science* **2001**, *291*, 2390.
(9) Heerbeek, R.; Kamer, P. C. J.; Leeuwen, P. W. N. M.; Reek, J. N. H. *Chem. Rev.* **2002**, *102*, 3717.
(10) Lee, M.; Cho, B.; Zin, W. *Chem. Rev.* **2001**, *101*, 3869.
(11) Thurn-Albrecht, T.; Schotter, J.; Kastle, G. A.; Emley, N.; Shibauchi, T.; Krusin-Elbaum, L.; Guarini, K.; Black, C. T.; Tuominen, M. T.; Russell, T. P. *Science* **2000**, *290*, 2126.
(12) Haruta, M. *Catal. Today* **1997**, *36*, 153.
(13) Lou, Y.; Maye, M. M.; Han, L.; Luo, J.; Zhong, C.-J. *Chem. Commun*. **2001**, 473.
(14) Kesavan, V.; Sivanand, P. S.; Chandrasekaran, S.; Koltypin, Y.; Gedanken, A. *Angew. Chem., Int. Ed. Engl.* **1999**, *38*, 3521.
(15) Nath, N.; Chilkoti, A. *Anal. Chem*. **2002**, *74*, 504.
(16) Katz, E.; Sheeney-Haj-Ichia, L.; Buckmann, A. F.; Willner, I. *Angew. Chem., Int. Ed.* **2002**, *41*, 1343.
(17) Park, S.; Taton, T. A.; Mirkin, C. A. *Science* **2002**, *295*, 1503.
(18) Kamat, P. V.; Barazzouk, S.; Hotchandani, S. *Angew. Chem., Int. Ed.* **2002**, *41*, 2764.
(19) Lahav, M.; Heleg-Shabtai, V.; Wasserman, J.; Katz, E.; Willner, I.; Durr, H.; Hu, Y.-Z.; Bossmann, S. H. *J. Am. Chem. Soc.* **2000**, *122*, 11480.
(20) Gittins, D. I.; Bethell, D.; Schiffrin, D. J.; Nichols, R. J. *Nature* **2000**, *408*, 67.
(21) Harrell, L. E.; Bigioni, T. P.; Cullen, W. G.; Whetten, R. L.; First, P. N. *J. Vac. Sci. Technol. B* **1999**, *17*, 2411.
(22) Musick, M. D.; Keating, C. D.; Keefe, M. H.; Natan, M. J. *Chem. Mater*. **1997**, *9*, 1499.
(23) Musick, M. D.; Pena, D. J.; Botsko, S. L.; McEvoy, T. M.; Richardson, J. N.; Natan, M. J. *Langmuir* **1999**, *15*, 844.
(24) Musick, M. D.; Keating, C. D.; Lyon, L. A.; Botsko, S. L.; Pena, D. J.; Holliway, W. D.; McEvoy, T. M.; Richardson, J. N.; Natan, M. J. *Chem. Mater*. **2000**, *12*, 2869.
(25) Shipway, A. N.; Lahav, M.; Blonder, R.; Willner, I. *Chem. Mater*. **1999**, *11*, 13.
(26) Shipway, A. N.; Willner, I. *Chem. Commun*. **2001**, 2035.
(27) Kolb, D. M. In *Advances in Electrochemistry and Electrochemical Engineering*; Gerischer, H., Tobias, C. W., Eds.; Wiley: New York, 1978; Vol. 11, pp 125−271.
(28) Hwang, S.; Oh, I.; Kwak, J. *J. Am. Chem. Soc*. **2001**, *123*, 7176.
(29) Michalitsch, R.; Laibinis, P. E. *Angew. Chem., Int. Ed.* **2001**, *40*, 941.
(30) Toshima, N.; Yonezawa, T. *New J. Chem*. **1998**, 1179.
(31) Adzic, R. In *Electrocatalysis*; Lipkowski, J., Ross, P. N., Eds.; Wiley-VCH: New York, 1998; p 197.
(32) Brust, M.; Bethell, D.; Kiely, C. J.; Schiffrin, D. J. *Langmuir* **1998**, *14*, 5425.
(33) Will, T.; Dietterle, M.; Kolb, D. M. In *Nanoscale Probes of the Solid−Liquid Interface*; Gewirth, A. A., Siegenthaler, H., Eds.; NATO ASI Series E.; Kluwer Academic: Dordrecht, 1995; Vol. 288, p 137.
(34) Handley, D. A. In *Colloidal Gold. Principles, Methods, and Applications*; Hayat, M. A., Eds.; Academic Press: New York, 1989; Vol. 1, p 13.
(35) Angerstein-Kozlowska, H.; Conway, B. E.; Hamelin, A.; Stoicoviciu, L. *J. Electroanal. Chem.* **1987**, *228*, 429.
(36) Shipway, A. N.; Katz, E.; Willner, I. *CHEMPHYSCHEM* **2000**, *1*, 18.
(37) Xu, B.; Tao, N. J. *Science* **2003**, *301*, 1221.
(38) Lu, M.; Li, X. H.; Yu, B. Z.; Li, H. L. *J. Colloid Interface Sci*. **2002**, *248*, 376.
(39) Swanson, T. *Natl. Bur. Stand. Circ*. **1953**, *539*, 133.
(40) Zanchet, D.; Hall, B. D.; Ugarte, D. *J. Phys. Chem. B* **2000**, *104*, 11013.
(41) Solov'eva, A.; Zhdanov, V. *Inorg. Mater*. **1985**, *21*, 828.
(42) Uosaki, K.; Shen, Y.; Kondo, T. *J. Phys. Chem*. **1995**, *99*, 14117.
(43) Kolb, D. M. *Angew. Chem., Int. Ed.* **2001**, *40*, 1162.
(44) Hagenstrom, H.; Schneeweiss, M. A.; Kolb, D. M. *Langmuir* **1999**, *15*, 7802.
(45) Hagenstrom, H.; Esplandiu, M. J.; Kolb, D. M. *Langmuir* **2001**, *17*, 839.
(46) Shimazu, K.; Kawaguchi, T.; Isomura, T. *J. Am. Chem. Soc*. **2002**, *124*, 652.
(47) Ingram, R. S.; Hostetler, M. J.; Murray, R. W. *J. Am. Chem. Soc.* **1997**, *119*, 9175.
(48) Long, J. W.; Stroud, R. M.; Swider-Lyons, K. E.; Rolison, D. R. *J. Phys. Chem. B* **2000**, *104*, 9772.
(49) Park, S.; Yang, P.; Corredor, P.; Weaver, M. J. *J. Am. Chem. Soc.* **2002**, *124*, 2428.
(50) Park, S.; Wieckowski, A.; Weaver, M. J. *J. Am. Chem. Soc*. **2003**, *125*, 2282.
(51) Solla-Gullon, J.; Montiel, V.; Aldaz, A.; Clavilier, J. *J. Electroanal. Chem.* **2000**, *491*, 69.
(52) Solla-Gullon, J.; Montiel, V.; Aldaz, A.; Clavilier, J. *J. Electrochem. Soc.* **2003**, *150*, E104.
(53) Lee, J.; Oh, I.; Hwang, S.; Kwak, J. *Langmuir* **2002**, *18*, 8025.
(54) Herrero, E.; Buller, L. J.; Abruna, H. D. *Chem. Rev.* **2001**, *101*, 1897.
(55) Michalitsch, R.; Palmer, B. J.; Laibinis, P. E. *Langmuir* **2000**, *16*, 6533.
(56) Hicks, J. F.; Miles, D. T.; Murray, R. W. *J. Am. Chem. Soc*. **2002**, *124*, 13322.
(57) Oh, I.; Gewirth, A. A.; Kwak, J. *Langmuir* **2001**, *17*, 3704.
(58) Oh, I.; Gewirth, A. A.; Kwak, J. *J. Catal*. **2003**, *213*, 17.
(59) Jennings, G. K.; Laibinis, P. E. *J. Am. Chem. Soc*. **1997**, *119*, 5208.
(60) Oyamatsu, D.; Kuwabata, S.; Yoneyama, H. *J. Electroanal. Chem*. **1999**, *473*, 59.
(61) Park, S.; Weaver, M. J. *J. Phys. Chem. B* **2002**, *106*, 8667.
(62) Shon, Y.-S.; Dawson, G. B.; Porter, M.; Murray, R. W. *Langmuir* **2002**, *18*, 3880.
(63) Moulder, J. F.; Stickle, W. F.; Sobol, P. E.; Bomben, K. D. *Handbook of X-ray Photoelectron Spectroscopy*; Phys. Elec. Inc.: Minnesota, 1995.
(64) Harikumar, K. R.; Ghosh, S.; Rao, C. N. R. *J. Phys. Chem. A* **1997**, *101*, 536.